

# Correlating topography and elastic properties of Elastin-Like Polypeptide scaffolds probed at the nanoscale: Intermodulation Atomic Force Microscopy experiments and Molecular Dynamic simulations

S. Trusso<sup>a</sup>, S. Firman<sup>b</sup>, J. Balasubramanian<sup>b</sup>, M. H. Khatami<sup>b</sup>, H. deHaan<sup>b</sup>, N. R. Agarwal<sup>b</sup>

<sup>a</sup>*CNR-Istituto per i Processi Chimico-Fisici, V.le F. Stagno d'Alcontres 37, Faro Superiore, 98158 Messina, Italy*

<sup>b</sup>*Faculty of Science, University of Ontario Institute of Technology, 2000 Simcoe Street North, Oshawa, ON L1H7K4, Canada.*

---

## Abstract

The synthesis and property characterization of soft biomaterials has taken precedence in recent years. Although bulk physical-chemical properties are well known for these bio-materials, nanoscale properties still need to be probed and evaluated to fine tune the bio-compatibility (structural as well as functional) with natural tissues for regenerative medicine, prosthetics and other biological applications. In this study, we focus on a popular soft bio-material, ELastin-like polypeptide (ELP) which has been prepared under different pH conditions. We explore the topographical features of the ELP at the nanoscale using Atomic Force Microscopy (AFM). Additionally, we employ a non linear mode of AFM called Intermodulation-AFM (ImAFM) to correlate the elastic properties (Young's modulus) of ELP probed at the nanoscale with the topographical features which gives us a deep insight into the mechanical properties offered by ELP when the structural features are

altered by change in the ELP synthesis conditions. The noteworthy point is that we measure these properties at a spatial resolution of 0.9 nm. Finally, we explain the change in the structural features of ELP with varying pH through atomistic Molecular Dynamics Simulations. We follow the interaction mechanisms of the amino acid sequences and crosslinkers with proteins as they form the backbone and sidechain of the ELP at different pH.

*Keywords:* Elastin-like Polypeptide, Intermodulation Atomic Force Microscopy, Mechanical Properties, Young Modulus, Nanoscale regime, Topography, Soft biomaterials

---

## 1. Introduction

The science of synthesizing biomaterials to enhance, support or replace damaged tissue or body functions is at least five decades old. They can either be natural or engineered to gear their function to specific needs. The development of biomaterial is a vital area in the fabrication of scaffolds. These engineered substrates are studied predominantly for their surface structural features correlating with cellular responses. The engineered substrates tend to be stiff and lack cell adhesive properties as compared to native extracellular matrix (ECM). Also, they are found to have angular and repetitive surface structures as compared to ECM that have undulating surfaces [1]. To overcome these differences in properties from native ECM, elastin-based material have been introduced into these engineered substrates since it is one of the most abundant protein found in native ECM [2]. Elastin is a protein that possesses inherent chemical resistance and high durability in entire body owing to the presence of more hydrophobic amino acids [3]. Elastin

16 acts as a main component to induce rubber-like elastic nature to the tis-  
17 sues, that support them by sustaining infinite deformation/relaxation cycles  
18 without getting ruptured [4]. This property of providing elastic recoil to stiff  
19 substrates makes elastin a better choice of material as a component in bioma-  
20 terial fabrication [5]. Additionally, elastin facilitates accelerated skin wound  
21 repair, enhances the proliferation of endothelial cells, vascular smooth muscle  
22 cells and skin fibroblast since it has the ability to interact with large number  
23 of cell surface receptors [6]. However, the extensive cross-linked structure  
24 and hydrophobic nature of elastin hinders the processing and fabrication of  
25 elastin into biomaterials [7]. Therefore, recombinant, synthetic and solu-  
26 ble forms of elastin like alpha-elastin, elastin-like polypeptides (ELPs) and  
27 tropoelastin are used to fabricate composites scaffolds [8].

28 Synthetic elastins such as ELPs belong to artificial peptide polymers class.  
29 The general composition of ELPs especially Val-Pro-Gly-X-Gly is a repeated  
30 unit of pentapeptide, where X can be any amino acid except proline. The  
31 Val-Pro-Gly-X-Gly domain is derived from tropoelastins hydrophobic domain  
32 [9]. ELPs are biodegradable and biocompatible. These ELPs exhibit lower  
33 critical solution temperature (LCST) phase behavior which results in insol-  
34 ule coacervate phase formation similar to tropoelastin [10]. The alteration  
35 of stimuli such as light, pH, concentration of salts and proteins can tune the  
36 LCST of ELPs. The stimuli-triggered self-assembly of ELPs can be achieved  
37 by their reversible phase behavior. The ELPs can also self assemble to form  
38 hydrogels [11] and nanoparticles [12] that act as potential candidates to use  
39 in drug delivery and tissue engineering applications [13, 14]. As an added  
40 advantage, the purification of ELPs without chromatography is easier owing

41 to its ability to undergo reversible phase separation when it exceeds tunable  
42 transition temperature [15].

43 The formation of hydrogel can be performed with proper peptide sequence  
44 and under specific aqueous conditions (*e.g.*, ionic strength, pH or tempera-  
45 ture) via a self-assembly technique [16]. These polypeptides adapt to form  
46 secondary structural  $\alpha$ -helices and  $\beta$ -sheets. This happens within peptide  
47 chains through intramolecular hydrogen bonding that renders specific con-  
48 formation based self-assembling nature and bioactivity. The polypeptide-  
49 based hydrogels have grabbed huge potential in biomedical applications ow-  
50 ing to structural similarity to ECM, enzyme biodegradability, cell adhesive  
51 properties and remarkable biocompatibility [17]. Moreover, the hydrogels  
52 can enhance cells adhesion, proliferation and differentiation and result in  
53 good bioactivity. The change in peptide length or replacement of amino  
54 acid residues is useful to alter the biological and physical properties of these  
55 hydrogels [18].

56 The common natural polymers (gelatin, collagen, pectin, gellan gum,  
57 chitosan and alginate) derived hydrogels also exhibit structural similarity to  
58 tissues, biocompatibility and good degradability. However, drawbacks con-  
59 cerning the suboptimal mechanical stability, immunogenic or inflammatory  
60 response still persists [19]. The application of hydrogel is mainly based on  
61 the mechanical properties of hydrogels. Indeed, the success and fate of the  
62 implant is purely based on the hydrogel mechanical properties that are com-  
63 patible with host tissue and is an important factor for consideration during  
64 design and fabrication of tissue regenerative systems. This should avoid the  
65 induced host inflammatory response [20]. The cellular responses are directed

66 by the extent of matrix stiffness [21]. The existence of mismatch in stiffness  
67 between native tissue and hydrogel often results in local stress that concen-  
68 trates at the interfaces. Also, the stress can be induced due to the lack of  
69 proper adhesion of the gel to the adjacent tissue that disturb relative mo-  
70 bility. The immune cell response by generation of pro-inflammatory signals  
71 can cause fibrosis and lead to shear stress [22]. Hence, hydrogels that usually  
72 exhibit less stiffness than the neighboring tissue could minimize the stress  
73 accumulation, and reduce formation of fibrous capsule. The peptide-based  
74 hydrogen biomaterials are appealing in areas of regenerative medicine and  
75 tissue engineering applications as they can adapt to the stiffness of tissue  
76 microenvironments *in vivo* [19].

77 The ELPs mechanical and topographical surface analysis plays a vital  
78 role in their development stage. In recent years, dynamic AFM technique  
79 has been extended to be driven with multiple frequencies as compared to  
80 traditional AFM where the cantilever is driven with a single frequency. Here,  
81 excitation of probe and measurement of response occurs at two or more fre-  
82 quencies which allow us to obtain more details on tip-surface interaction [23].  
83 One of the multi-frequency dynamic AFM method is Intermodulation AFM  
84 (ImAFM) that employs for capturing of several frequency mixing products  
85 by two driving frequencies closer to single frequency cantilever resonance in-  
86 stead of higher eigenmodes or higher harmonics excitation of the cantilever  
87 [24]. In ImAFM, same thermal noise measurement is applied to calibrate  
88 both the cantilever and deflection sensor. ImAFM is capable of measuring  
89 the tip-surface force accurately as a function of the cantilever deflection using  
90 this calibration. The route to map the materials elastic response and local

91 viscous nature arise from the possibility to measure how both the dissipative  
92 and conservative components of the interaction depends on the amplitude of  
93 oscillatory motion [25].

94 In this study, we validate the ImAFM technique by measuring the effective  
95 elastic properties i.e. Young's modulus of ELP at the nanoscale in spacings of  
96 1 nm and correlate them with topographical features. The ELP biomaterial  
97 were synthesized at different pH conditions to observe the change in their  
98 nanoscopic structural features and their relative elastic behavior. We also  
99 explain the underlying mechanisms for different structural properties of ELP  
100 at different pH through Molecular Dynamic simulations.

## 101 **2. Experimental section**

### 102 *2.1. Elastin-like Polypeptide (ELP) production and purification*

103 The construction of the plasmid, the expression of ELP in escherichia coli  
104 and the following purification steps have been described in detail elsewhere[1].  
105 Shortly, the pET15b plasmid containing the ELP sequence was transformed  
106 with a heatshock at 42°C into competent BL21-PLyS e.coli (Invitrogen).  
107 The ELP contained either a fibronectin cell binding site (RGD) or a scram-  
108 bled version of that amino sequence (RDG). The transformed bacteria were  
109 cultured in terrific broth containing 100  $\mu\text{g}/\text{ml}$  ampicillin until an optical  
110 density of 0.8 at 600 nm has been reached, at which point protein expression  
111 was induced with 1 mM isopropyl  $\beta$ -D-1-thiogalactopyranoside. After 5-7 h  
112 of expression, the cells were lysed by freeze-thaw cycles with the addition of  
113 DNase and 1 mM phenylmethylsulphonyl fluoride. From there the protein  
114 was recovered by iterative inverse temperature cycling. As a final step, the

115 protein is dialyzed three times through a 3.5 kDa membrane at 4°C and then  
116 lyophilized.

## 117 *2.2. Intermodulation Atomic Force Microscopy*

118 The surface morphology of the films produced was imaged by an Atomic  
119 Force Microscope (AFM) by NT-MDT working in tapping mode. Images  
120 of the sample surface were acquired on a  $5 \times 5 \mu\text{m}^2$  area using silicon can-  
121 tilever from Nanosensors (type NCH-50), working at the resonance frequency  
122  $f=362\text{KHz}$ , tip radius  $r < 10 \text{ nm}$ , quality factor of  $Q=490$ , and force con-  
123 stant  $34.4 \text{ N/m}$ . During the acquisition of the samples surface topography  
124 their elastic properties were acquired using the intermodulation technique.  
125 In a standard AFM measurement, the tip is driven at its resonance frequency  
126 where the tip oscillation amplitude and phase gather information of the topo-  
127 graphical features and nature of the investigated material. A linear response  
128 of the tip at the driving frequency is assumed. However, the behaviour of  
129 the tip motion is highly non linear when the tip interacts with the sample  
130 surface.

131 Measurements were performed with pixel dimensions of  $512 \times 512$  on  
132 areas of  $5 \times 5 \mu\text{m}^2$  giving us a spatial resolution of about  $0.9 \text{ nm}$ . Within  
133 the same intermodulation measurement both the surface topography and the  
134 force curves were obtained for each scanned point. The value of the elastic  
135 modulus was then obtained by performing the fitting procedure with the  
136 modified DMT model to the force curve as analyzed from the inversion of  
137 the intermodulation signals. The fitting procedure is performed within the  
138 IMP software suite at each point of the scanned surface.

139 *2.3. MD simulation details*

140 We run all-atom molecular dynamics (MD) simulations of elastin-like  
141 polypeptide (ELP) system. Our system contains cell-binding (TVYAVT-  
142 GRGDSPASSAA) and structural domains ((VPGIG)2VPGKG(VPGIG)2)3,  
143 QK peptides (KKLTWQELYQL[K(Ac)]Y[K(Ac)]GI), and THPC, TrHP and  
144 TrHPO ligands as cross-linkers. Here we use GROMACS 2016.4 package to  
145 run our MD simulations, using CHARMM36 force field. We run three simu-  
146 lations to mimic the system at three different pH values: pH 5, 7, and 9. The  
147 only amino acid in the range that could be affected by the change of pH in  
148 this range are HIS and CYS[30]. Thus, based on the amino acids in our ELP,  
149 the pH range that is introduced to our system does not affect the charge of  
150 the proteins. However, the change in the pH affects the properties of cross-  
151 linkers in the system. At lower pH values (pH 5), the only cross-linkers in  
152 the system are THPC, while at higher pH values THPC changes into TrHP  
153 and TrHPO ligands (Fig.1)[31, 32, 33, 34]. The content of each system could  
154 be found in Table 1. Each simulation box contains 9 cell binding and struc-  
155 tural domain peptides, 16 QK peptides and 200 cross-linkers. At pH 5, all  
156 of our cross-linkers are THPC molecules, at pH 7 THPC, TrHP and TrHPO  
157 ligands co-exist (1:2:1 ratio) as our cross-linkers and in pH 9, only TrHP and  
158 TrHPO ligands (3:2 ratio) are present. Cl counterions are used to neutralize  
159 our system and TIP3P water molecules are used to solvate the simulation  
160 box (Table 1).

161 The same approach is used to set up and run our simulations for all  
162 three systems. After energy minimization, under NVT conditions (NVT: a  
163 canonical ensemble, where the number of particles (N), the volume of the

Table 1: System content for each simulation at different pH values

Simulation box content	pH5	pH7	pH9
Cell and structural binding	9	9	9
QK-peptide	16	16	16
THPC	200	50	-
TrHP	-	100	120
TrHPO	-	50	80
Cl <sup>-</sup>	243	93	43
TIP3P	45270	45661	45824

164 system (V) and the temperature of the system (T) remains constant) we  
 165 run brief MD simulation at T=300 K using Nose-Hoover thermostat for 2  
 166 ns with time steps of 1 fs. Protein positions are restrained in this step to  
 167 prevent any dramatic structural changes before the production run. Next,  
 168 we run a brief simulation under NPT condition (NPT: an isothermalisobaric  
 169 ensemble, where the number of particles (N), the pressure of the system (P)  
 170 and the temperature of the system (T) remains constant) at T=300 K, and  
 171 pressure=1 atm, using Parrinello-Rahman and isotropic pressure coupling,  
 172 with  $\tau_p=5$  ps and compressibility =  $4.5 \times 10^{-5} \text{bar}^{-1}$  for 100ps with time steps  
 173 of 2fs, keeping the protein positions restrained. After this short simulation,  
 174 we start the production run under NPT conditions and using the same con-  
 175 ditions as the previous step, without position restraints for 400 ns. Visual  
 176 Molecular Dynamics (VMD) package and customized C++ codes are used  
 177 to calculate our results. VMD is also used to visualize our structures.

178 **3. Results and Discussion**

179 *3.1. Elastic Properties Modeling*

180 The elastic properties of the ELP surface were obtained by modelling  
181 the contact mechanism of the AFM probe with the samples surface using  
182 the Derjaguin-Muller-Toropov (DMT) model [26], a model suitable in cases  
183 where there is low adhesion force and small tip radii. The reconstructed force  
184 curves  $F(z)$ , where  $z$  is the tip to surface distance, obtained from the non  
185 linear analysis of the tip motion [27, 28] can be modeled by the following  
186 relations:

$$F(z) := \begin{cases} -F_{min} \frac{a_0^2}{(z+a_0)^2} - k_{long}d & z > -h \\ -F_{min} + \frac{4}{3}E^* \sqrt{-Rz^3} - k_{long}d & z < -h \end{cases} \quad (1)$$

187 where  $h$  is the tip equilibrium position above the surface,  $F_{min}$  is the minimum  
188 of the force,  $a_0$  is the intermolecular distance,  $R$  is tip radius and  $k_{long}$  is an  
189 additional parameter introduced in the DMT model which takes into account  
190 long distance interaction force between the tip and the sample surface. As an  
191 example, in Fig.2 we report the results of the fitting procedure with the DMT  
192 model to the experimental curve obtained at a given point on the surface of  
193 the ELP sample synthesized at pH3. As it can be seen the different regimes  
194 *e.g.* the attractive and repulsive regions of the force-distance curve, *e.g.* when  
195 the tip is not in contact and after the contact are well reproduced. The elastic  
196 modulus  $E^*$  obtained by the fit in this case was of 0.98 GPa.

197 *3.2. Atomic Force Microscopy*

198 The morphology represented by the ELP at microscopic scales are 'bead  
199 and string' like features [29]. When measuring these features with AFM,

200 we observe the beads to be bigger than their probable size while the strings  
201 are not visualized at all. In Fig.3 are presented the surface topography of  
202 the samples grown at pH3, pH6 and pH9 respectively. This is due to the  
203 resolution of the AFM which is presented by the tip while it scans the sample.  
204 As it can be clearly seen, the surface morphology presents marked differences  
205 as a function of the pH value. The surface of the pH3 sample is very smooth  
206 when observed at short distances, however it shows strong variations of the  
207 surface height along distances of the  $\mu m$  order. In fact, a height variation of  
208 about  $2 \mu m$  is observed along a surface distance of  $5 \mu m$ . As the pH values  
209 increases, a different behaviour is observed: at long distances the surface  
210 topography seems to become more flat but at the same time height variation  
211 at short distances increases. In order to highlight this behaviour in Fig.4 we  
212 report the surface profiles collected along a line on the surface of the samples.  
213 As it can be clearly seen the bead size of ELP decreases as we move to higher  
214 pH hence the image for pH9 shows a smoother surface compared to the image  
215 for pH3.

### 216 3.3. *Elastic modulus*

217 In Fig.5 are shown the map of the elastic modulus obtained by fitting  
218 the force curves resulting from the intermodulation measurements at each  
219 point of the samples surface. The value of  $E^*$  is within the 0-1.2 GPa range  
220 for all the samples. Nevertheless null or very low  $E^*$  values usually corre-  
221 spond to surface points where the force curve could not be properly fitted by  
222 the DMT model, probably the consequence of a bad tip-surface interaction.  
223 Looking at the maps in Fig.5 the details of the surface topography can be  
224 clearly observed, pointing out how the surface morphology, and hence the

225 pH value plays a role in determining the elastic properties of the samples.  
226 However, a clear picture of the  $E^*$  dependence on pH does not emerge from  
227 the maps. To this purpose we report in Fig.6 the histogram of distribu-  
228 tion of the elastic modulus in the investigated areas for ELP synthesized at  
229 different pH. Looking at the  $E^*$  distribution function for the pH3 prepared  
230 sample, a continuous distribution of values between 0 and 1.2 GPa is ob-  
231 served. Nevertheless three maxima are present: the first peaked at  $E^*=0$ ,  
232 whose probable origin has been discussed earlier, the second at about 0.21  
233 GPa and the third at about 0.6-0.7 GPa. The second and third region can  
234 be regarded as *soft* and relatively *hard* components respectively. It worth  
235 noticing that a continuous tail extends till the maximum observed value .  
236 The elastic modulus distribution of the samples prepared at pH6 and pH9  
237 show a similar behaviour, with the exception of the drastic decrease of the  
238 values around 0 GPa, pointing out how the different sample morphologies  
239 lead to a better tip-surface interaction as long as the surface become more  
240 *flat*. Also for these samples two maxima are present in the  $E^*$  frequency  
241 distribution peaked at 0.3 and 0.7 GPa, confirming the observation of a *soft*  
242 and the relatively *hard* phases. Thus, a well defined two-phase structure,  
243 *soft* and *hard*, emerges in the elastic properties of the ELP as long as the  
244 pH value is increased above pH3. The origin and the molecular structure  
245 of these two phases cannot be easily individuated solely on the basis of the  
246 AFM and ImAFM measurements. In order to understand the evolution of  
247 the ELP structure at a microscopic level as a function of the pH values, we  
248 performed molecular dynamic simulations of the ELP system to understand  
249 the underlying mechanisms for change in structural behavior at varying pH.

250 *3.4. Role of pH on the micro-structural properties of the ELP explained by*  
251 *MD simulations*

252 *3.4.1. General Interaction with Proteins*

253 Figure 7 indicates the general initial configuration of our system at pH  
254 7 and final configuration for pH 5, pH 7, and pH 9. We can see that in  
255 all systems, the proteins self-assemble and interact with the cross-linkers.  
256 Moreover, in each system, we have cross-linkers floating in the water, which  
257 indicates the possibility of these molecules to solubilize in water.

258 Our results indicate that the number of contacts between proteins and  
259 the cross-linkers in the system is pH dependent (Fig.8A). At pH 5 we have  
260 the least amount of interactions between the cross-linkers (THPC) and the  
261 protein units, while at pH 7 this value is increased by more than twice be-  
262 tween the mixture of the cross-linkers (THPC, TrHP, and TrHPO) and the  
263 proteins. At pH 9 the number of interactions is slightly higher than pH 7.  
264 At this pH, the mixture of cross-linkers contains TrHP and TrHPO. Based  
265 on the results obtained in our simulations, we do not see any major change  
266 in the interactions during the last 200 ns of the simulations. Thus, we have  
267 used the last 200 ns of the trajectory for calculating the rest of our results  
268 in this paper unless stated otherwise.

269 *3.4.2. Detailed Interactions with amino acids*

270 **pH5:** At pH 5, we can see that 30% of THPC cross-linkers interact with  
271 the protein (Fig.8B). Similarly, at pH 7, around 30% of THPC is interacting  
272 with proteins, while more than 50% of TrHPO and 80% of TrHP is interact-  
273 ing with protein (Fig.8C). At pH 9 TrHPO and TrHP are interacting with  
274 proteins at almost the same ratio as the pH 7 system (Fig.8D). Different

275 cross-linkers interact with different residues on the proteins. At pH 5, THPC  
276 is mainly interacting with ASP and GLU, which are both negatively charged  
277 (Fig.9A). This is compatible with the general view that THPC has a positive  
278 charge, and thus interacts with negatively charged residues, based on the  
279 electrostatic interactions. Here, we can see that THPC is mainly interacting  
280 with side chains of the ASP and GLU. More generally, THPC is mainly in-  
281 teracting with the sidechain of negatively charged or polar residues, while for  
282 positively charged or non-polar residues, such as ILE, THPC interacts with  
283 the backbone of the residue.

284 **pH7:** At pH 7, we can see that THPC is mainly interacting with GLU,  
285 ASP (similar to the pH 5 system), which are both negatively charged, GLN,  
286 which is polar with partial negative charge and ARG, which is positively  
287 charged (Fig. 10). More detailed studies indicate that in the case of ARG,  
288 THPC is interacting with the backbone part of the amino acid. In this pH,  
289 THPC is mainly interacting with the sidechain of the negatively charged  
290 residues and polar residues, similar to the pH 5 system (Fig.10B). The two  
291 exceptions are TYR, and ALY (acetylated LYS). First, THPC is mainly in-  
292 teracting with the backbone of TYR at pH 7, unlike pH 5. Second, THPC  
293 is mainly interacting with the side chain of ALY, where the amino acid has  
294 partial negative charge. In the case of TrHP, the molecule interacts with a  
295 variety of charged, polar and non-polar residues, without any main prefer-  
296 ence. However, the interactions with charged or polar residues are mainly  
297 through sidechains, while for non-polar residues the interactions are mainly  
298 through the backbone (Fig.10C). We can see that TrHP has significant inter-  
299 action with the sidechain of positively charged residues compared to THPC.

300 TrHPO has generally much higher interactions with charged residues com-  
301 pared to the other cross-linkers, especially in the case of interacting with  
302 LYS (Fig. 10A). Similar to THPC and TrHP, TrHPO interacts with the po-  
303 lar and charged amino acids mainly through the sidechain, and for non-polar  
304 residues, the TrHPO mainly interacts with the backbone region (Fig. 10D).

305 **pH9:** At pH 9, TrHP and TrHPO have similar interaction with the amino  
306 acids in the system (Fig. 11). These patterns are also similar to the patterns  
307 of TrHP and TrHPO at pH 7 (Fig. 10). Here, we can see that both cross-  
308 linkers have higher interactions with charged and polar residues, and these  
309 interactions mainly occur with the side chain of the amino-acids (Fig. 11B  
310 and C).

### 311 *3.4.3. Interaction with the backbone*

312 We can see in Fig. 12 that in the case of interaction with the backbone, all  
313 cross-linkers mainly interact with the CO group of the backbone, which has  
314 the highest electronegativity. NH group has much less interaction compared  
315 to CO group, while the  $C_\alpha$  has the lowest interaction with cross-linkers in  
316 the backbone.

### 317 *3.4.4. Interaction with proteins*

318 Figure 13 indicates the normalized share of interaction between cross-  
319 linkers and the protein. We can see that the cross linkers have more normal-  
320 ized interactions with QK peptides in the system. Figure 14 indicates the  
321 higher number of interactions between cross-linkers and proteins in higher  
322 pH values. Moreover, these results indicate higher interaction between QK  
323 peptides and the cross-linkers in all pH values.

324 Based on our simulations, proteins do aggregate, while the cross-linkers  
325 covers the outer area of the protein chunks and produce some domain-like  
326 configurations (Figure 15). At lower pH values, a lower number of cross-  
327 linkers cover protein surface. Thus, the domains could diffuse and produce  
328 larger domains with similar properties. However, at higher pH values, the  
329 higher surface density of the crosslinkers prevents the protein domains to  
330 diffuse and hence the bead size reduces.

#### 331 **4. Conclusion**

332 We were able to successfully analyze the elastic properties at the nanoscale  
333 of soft biomaterials, ELP in our study, probed by AFM tip using the ImAFM.  
334 ImAFM has proven its capabilities to measure the visco-elastic properties of  
335 soft materials as a new mode of AFM technique. In particular, we measure  
336 the elastic properties of the proteins and not of crosslinkers. The spatial  
337 resolution offered by ImAFM to evaluate the elastic properties is about 0.9  
338 nm. Hence, we see that the elastic values at different pH values remain  
339 the same. The domain size dependent on pH does not change the Youngs  
340 modulus value as can be seen in the scale bar (range: 0 - 1.8 GPa) of the  
341 figures with different pH.

342 Our simulations reach energetically feasible configuration after 200ns of  
343 simulations. These simulations indicate direct relation of pH dependency  
344 in ELP systems. Since THPC is positively charged, in all simulations it  
345 mainly interacts with negatively charged residues, through electrostatic in-  
346 teractions. TrHPO mainly interacts with polar and charged residues (both  
347 positive and negative). This is due to the neutral charge and the P=O bond,

348 which provides strong H-bond interactions with these residues. TrHP has  
349 the highest normalized number of interactions with ELP, which is due to the  
350 non-polar region in the center of the particle and O-H groups on the chains  
351 which provides both polar and non-polar interaction with ELP. In terms of  
352 interaction with LYS, TrHPO has the highest interaction, while TrHP has  
353 lower interaction and THPC does not interact.

## 354 **5. Acknowledgements**

355 We would like to thank the Natural Sciences and Engineering Research  
356 Council of Canada (NSERC) for financial support. The authors are also  
357 thankful to Dr. Salvatore Patane for his expertise and providing us with  
358 the right stiffness tips from Nanosensors (type NCH-50) to carry out the  
359 Intermodulation-AFM experiments. Dr. Agarwal and Dr. Trusso would also  
360 like to acknowledge the support of Dr. Daniel Forchheimer and Dr. Erik  
361 Tholen for setting-up the Intermodulation system on the NT-MDT AFM  
362 hardware. Finally, Dr. Agarwal is grateful to Dr. Alexandra Paul for prepa-  
363 ration of the ELP samples at varying pH.

## 364 **6. References**

- 365 [1] A. Paul, M. Sthrenberg, S. Chen, D. Rhee, W.-K. Lee, T. Odom, S.  
366 Heilshorn, A. Enejder, Micro-and nano-patterned elastin-like polypep-  
367 tide hydrogels for stem cell culture, *Soft Matter*, 13 (2017) 5665-5675.
- 368 [2] Z. Chen, Q. Zhang, H. Li, Q. Wei, X. Zhao, F. Chen, Elastin-like  
369 polypeptide modified silk fibroin porous scaffold promotes osteochon-  
370 dral repair, *Bioactive materials*, 6 (2021) 589-601.

- 371 [3] W. Kim, E.L. Chaikof, Recombinant elastin-mimetic biomaterials:  
372 emerging applications in medicine, *Advanced drug delivery reviews*, 62  
373 (2010) 1468-1478.
- 374 [4] F.W. Keeley, C.M. Bellingham, K.A. Woodhouse, Elastin as a selfor-  
375 ganizing biomaterial: use of recombinantly expressed human elastin  
376 polypeptides as a model for investigations of structure and selfassembly  
377 of elastin, *Philosophical Transactions of the Royal Society of London.*  
378 *Series B: Biological Sciences*, 357 (2002) 185-189.
- 379 [5] B. Gurumurthy, P.C. Bierdeman, A.V. Janorkar, Composition of elastin  
380 like polypeptidecollagen composite scaffold influences in vitro osteogenic  
381 activity of human adipose derived stem cells, *Dental Materials*, 32 (2016)  
382 1270-1280.
- 383 [6] S. Hinderer, S.L. Layland, K. Schenke-Layland, ECM and ECM-like ma-  
384 terialsBiomaterials for applications in regenerative medicine and cancer  
385 therapy, *Advanced drug delivery reviews*, 97 (2016) 260-269.
- 386 [7] W. Daamen, T. Hafmans, J. Veerkamp, T. Van Kuppevelt, Comparison  
387 of five procedures for the purification of insoluble elastin, *Biomaterials*,  
388 22 (2001) 1997-2005.
- 389 [8] D. Miranda-Nieves, E.L. Chaikof, Collagen and elastin biomaterials for  
390 the fabrication of engineered living tissues, *ACS Biomaterials Science &*  
391 *Engineering*, 3 (2017) 694-711.
- 392 [9] V.P. Vaikari, M. Park, L. Keossayan, J.A. MacKay, H. Alachkar,  
393 Anti-CD99 scFv-ELP nanoworms for the treatment of acute myeloid

- 394 leukemia, *Nanomedicine: Nanotechnology, Biology and Medicine*, 29  
395 (2020) 102236.
- 396 [10] D. Zhu, H. Wang, P. Trinh, S.C. Heilshorn, F. Yang, Elastin-like protein-  
397 hyaluronic acid (ELP-HA) hydrogels with decoupled mechanical and  
398 biochemical cues for cartilage regeneration, *Biomaterials*, 127 (2017)  
399 132-140.
- 400 [11] L. Martn, M. Alonso, A. Girotti, F.J. Arias, J.C. Rodriguez-Cabello,  
401 Synthesis and characterization of macroporous thermosensitive hydro-  
402 gels from recombinant elastin-like polymers, *Biomacromolecules*, 10  
403 (2009) 3015-3022.
- 404 [12] J.R. McDaniel, I. Weitzhandler, S. Prevost, K.B. Vargo, M.-S. Appavou,  
405 D.A. Hammer, M. Gradzielski, A. Chilkoti, Noncanonical self-assembly  
406 of highly asymmetric genetically encoded polypeptide amphiphiles into  
407 cylindrical micelles, *Nano letters*, 14 (2014) 6590-6598.
- 408 [13] E.E. Fletcher, D. Yan, A.A. Kosiba, Y. Zhou, H. Shi, Biotechnological  
409 applications of elastin-like polypeptides and the inverse transition cycle  
410 in the pharmaceutical industry, *Protein expression and purification*, 153  
411 (2019) 114-120.
- 412 [14] S. Roberts, M. Dzuricky, A. Chilkoti, Elastin-like polypeptides as models  
413 of intrinsically disordered proteins, *FEBS letters*, 589 (2015) 2477-2486.
- 414 [15] T. Christensen, M. Amiram, S. Dagher, K. TrabbicCarlson, M.F.  
415 Shamji, L.A. Setton, A. Chilkoti, Fusion order controls expression level

- 416 and activity of elastinlike polypeptide fusion proteins, *Protein Science*,  
417 18 (2009) 1377-1387.
- 418 [16] H.J. Kang, S. Kumar, A. D’Elia, B. Dash, V. Nanda, H.C. Hsia, M.L.  
419 Yarmush, F. Berthiaume, Self-assembled elastin-like polypeptide fusion  
420 protein coacervates as competitive inhibitors of advanced glycation end-  
421 products enhance diabetic wound healing, *Journal of Controlled Release*,  
422 333 (2021) 176-187.
- 423 [17] K.J. Hogan, A.G. Mikos, Biodegradable thermoresponsive polymers:  
424 Applications in drug delivery and tissue engineering, *Polymer*, 211  
425 (2020) 123063.
- 426 [18] X. Ding, H. Zhao, Y. Li, A.L. Lee, Z. Li, M. Fu, C. Li, Y.Y. Yang, P.  
427 Yuan, Synthetic peptide hydrogels as 3D scaffolds for tissue engineering,  
428 *Advanced drug delivery reviews*, (2020).
- 429 [19] E. Zeimaran, S. Pourshahrestani, A. Fathi, N.A. bin Abd Razak, N.A.  
430 Kadri, A. Sheikhi, F. Baino, Advances in bioactive glass-containing in-  
431 jectable hydrogel biomaterials for tissue regeneration, *Acta Biomateri-*  
432 *alia*, (2021).
- 433 [20] S.A. Young, H. Riahinezhad, B.G. Amsden, In situ-forming, mechani-  
434 cally resilient hydrogels for cell delivery, *Journal of Materials Chemistry*  
435 *B*, 7 (2019) 5742-5761.
- 436 [21] R.K. Das, V. Gocheva, R. Hammink, O.F. Zouani, A.E. Rowan, Stress-  
437 stiffening-mediated stem-cell commitment switch in soft responsive hy-  
438 drogels, *Nature materials*, 15 (2016) 318-325.

- 439 [22] R. Klopffleisch, F. Jung, The pathology of the foreign body reaction  
440 against biomaterials, *Journal of biomedical materials research Part A*,  
441 105 (2017) 927-940.
- 442 [23] R. Garcia, E.T. Herruzo, The emergence of multifrequency force mi-  
443 croscopy, *Nature nanotechnology*, 7 (2012) 217.
- 444 [24] D. Platz, E.A. Tholn, D. Pesen, D.B. Haviland, Intermodulation atomic  
445 force microscopy, *Applied Physics Letters*, 92 (2008) 153106.
- 446 [25] H. Huang, I. Dobryden, P.-A. Thorn, L. Ejenstam, J. Pan, M. Fielden,  
447 D. Haviland, P.M. Claesson, Local surface mechanical properties of  
448 PDMS-silica nanocomposite probed with Intermodulation AFM, *Com-  
449 posites Science and Technology*, 150 (2017) 111-119.
- 450 [26] B.V. Deriaguin, V.M. Muller, Y.P. Toporov, Effect of contact deforma-  
451 tion on the adhesion of particles, *J. Coll. Interf. Sci.* **53**, 314 (1975).
- 452 [27] D. Forchheimer, D. Platz, E. Tholén, B.B. Haviland, Model-based  
453 extraction of material properties in multifrequency atomic force mi-  
454 croscopy, *Phys. Rev. B*, **85**, 195449 (2012).
- 455 [28] S.S. Borysov, D. Platz, A.S de Wijn, D. Forchheimer, E. Tholén, A.V.  
456 Balatsky, B.B. Haviland, Reconstruction of tip-surface interactions with  
457 multimodal intermodulation atomic force microscopy, *Phys. Rev., B* **88**,  
458 115405 (2013).
- 459 [29] H. Wang, A. Paul, D. Nguyen, A. Enejder, S.C. Heilshorn, Tunable Con-  
460 trol of Hydrogel Microstructure by Kinetic Competition between Self-

- 461 Assembly and Crosslinking of Elastin-like Proteins, ACS Appl. Mater.  
462 Interfaces. **10**, 21808 (2018).
- 463 [30] D. L. Nelson and M. M. Cox, Lehninger Principles of Biochemistry, New  
464 York: Worth Publishers, 2000.
- 465 [31] D. A. Handley, in Colloidal Gold: Principles, Methods and Applications,  
466 ed. M. A. Hayat, Academic, San Diego, CA, 1989.
- 467 [32] Frank, A. W., & Drake, G. L. (1973). The Iodometric Determination  
468 of P(III) in Flame Retardants for Cotton: Part I: Development of the  
469 Method. Textile Research Journal, **43** 633638.
- 470 [33] M. Grayson (1963). Phosphonium Compounds. III. Mechanism of Hy-  
471 droxide Cleavage of Tetrakis(hydroxymethyl)phosphonium Chloride.  
472 Journal of the American Chemical Society, **85** 7983.
- 473 [34] S. X. Shao, L. Jiang, Li, Y. Li, Q. K. Shi (2012) Effect of pH on the  
474 Phosphorous Components in Tetra-Hydroxymethyl Phosphonium Chlo-  
475 ride Solution. Advanced Materials Research, 237241.

476 **List of Figures**

477 1 The structures of A) tetra-hydroxymethyl phosphonium chlo-  
478 ride (THPC), B) tri-hydroxymethyl phosphine (TrHP), C) tri-  
479 hydroxymethyl phosphine oxide (TrHPO). . . . . 26

480 2 Force-deflection curve acquired on the surface of the pH3 ELP  
481 sample. The red curve is the result of the fitting procedure  
482 using Eq.1. . . . . 27

483 3 AFM images (scan area  $5\mu\text{m} \times 5\mu\text{m}$  ) of the surfaces of the ELP  
484 sample prepared at a) pH3, b) pH6 and c) pH9. . . . . 28

485 4 Line profile along the surface of the ELP samples produced at  
486 different pH values. . . . . 29

487 5 Maps of the elastic modulus  $E^*$  obtained fitting the force  
488 curves using the DMT model. Maps in panel a), b) and c)  
489 correspond to the scanned areas reported in Fig.3. . . . . 30

490 6 Histogram of distribution function of elastic modulus for ELP  
491 synthesized for different pH 3, 6 and 9 . . . . . 31

492 7 A) Top and B) side view of the initial configuration of the  
493 system for pH 7. The protein content and position are the  
494 same for all three pH value systems. The cell binding and  
495 structural binding sites are covalently connected. The initial  
496 configuration of proteins is set to  $\alpha$ -helical configuration. Cell  
497 binding peptides are in orange, structural binding peptides are  
498 in blue and QK peptides are in red. LYS amino acids are in  
499 green. THPC is in purple, TrHP is in orange and TrHPO is  
500 in tan. . . . . 32

501 8 Interactions between the cross-linkers and proteins. A) Num-  
502 ber of total contacts at different pH values, B) percent of  
503 THPC crosslinkers interacting with proteins at pH5, C) per-  
504 cent of different crosslinkers interacting with proteins at pH  
505 7 and D) percent of different crosslinkers interacting with pro-  
506 teins at pH9. . . . . 33

507	9	Cross-linkers at pH 5 interacting with different amino acids of	
508		the protein mixture. A) Number of contacts between THPC	
509		cross-linkers and different amino acids residues in the system	
510		and B) ratio of THPC interacting with the side chain vs back-	
511		bone of each amino acid. The values in (A) are normalized by	
512		the number of amino acids in the system and the number of	
513		cross-linkers in the system. . . . .	34
514	10	Cross-linkers at pH 7 interacting with different amino acids of	
515		the protein mixture. A) Number of contacts between THPC,	
516		TrHP and TrHPO cross-linkers and different amino acids residues	
517		in the system, B) ratio of THPC interacting with the side chain	
518		vs backbone of each amino acid, C) ratio of TrHP interacting	
519		with the side chain vs backbone of each amino acid and D)	
520		ratio of TrHPO interacting with the side chain vs backbone	
521		of each amino acid. The values in (A) are normalized by the	
522		number of amino acids in the system and the number of cross-	
523		linkers in the system. . . . .	35
524	11	Cross-linkers at pH 9 interacting with different amino acids of	
525		the protein mixture. A) Number of contacts between TrHP	
526		and TrHPO cross-linkers and different amino acids residues in	
527		the system, B) ratio of TrHP interacting with the side chain	
528		vs backbone of each amino acid and C) ratio of TrHPO in-	
529		teracting with the side chain vs backbone of each amino acid.	
530		The values in (A) are normalized by the number of each amino	
531		acids in the system and the number of cross-linkers in the system.	36
532	12	Number of contacts between different cross-linkers with differ-	
533		ent parts of protein backbone in different pH values. A) pH5,	
534		B) pH7 and C) pH9. Number of contacts are normalized by	
535		total number of the cross-linker. . . . .	37
536	13	Number of contacts between different cross-linkers and differ-	
537		ent proteins in the system at different pH values. A) pH5,	
538		B) pH7 and C) pH9. Each cross-linker interaction is normal-	
539		ized by total number of the cross-linker. For each peptide, the	
540		number of interactions is normalized by number of the same	
541		type peptides, as well as the number of amino acids on each	
542		peptide. . . . .	38

543	14	Number of contacts between all cross-linkers and different proteins in the system at different pH values. The values are normalized by total number of the cross-linkers and total the number of amino acids on each peptide. . . . .	39
544			
545			
546			
547	15	Schematics on the role of cross-linkers and proteins in producing the ELP configurations in different pH values. At low pH values (A), lower number of cross-linkers have covered the protein, while at higher pH values, (B) a greater number of cross-linkers have covered the protein. The aggregated proteins are shown as purple circles. The cross-linkers are shown as cross sign in different colors.. . . .	40
548			
549			
550			
551			
552			
553			

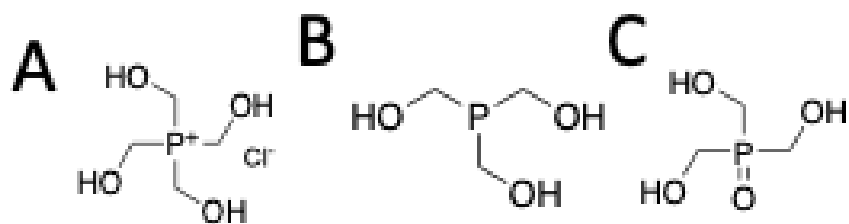


Figure 1: The structures of A) tetra-hydroxymethyl phosphonium chloride (THPC), B) tri-hydroxymethyl phosphine (TrHP), C) tri-hydroxymethyl phosphine oxide (TrHPO).

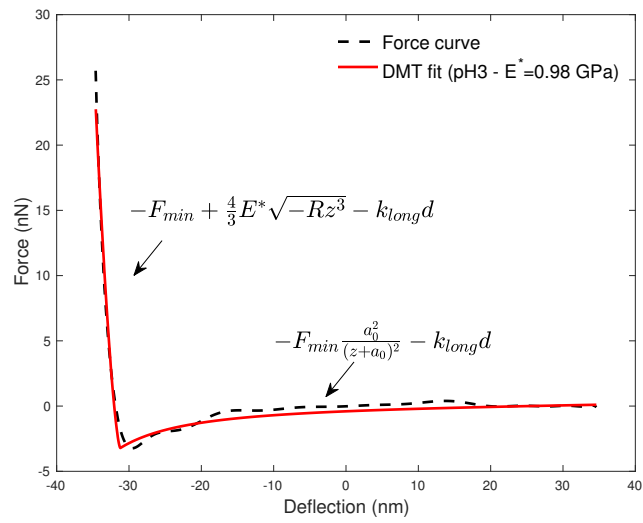


Figure 2: Force-deflection curve acquired on the surface of the pH3 ELP sample. The red curve is the result of the fitting procedure using Eq.1.

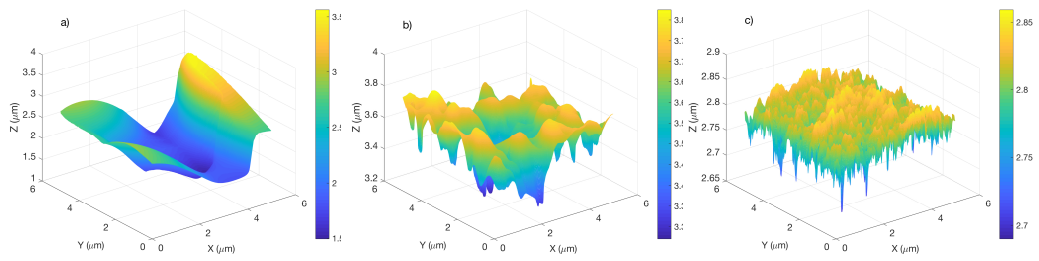


Figure 3: AFM images (scan area  $5\mu\text{m}\times 5\mu\text{m}$ ) of the surfaces of the ELP sample prepared at a) pH3, b) pH6 and c) pH9.

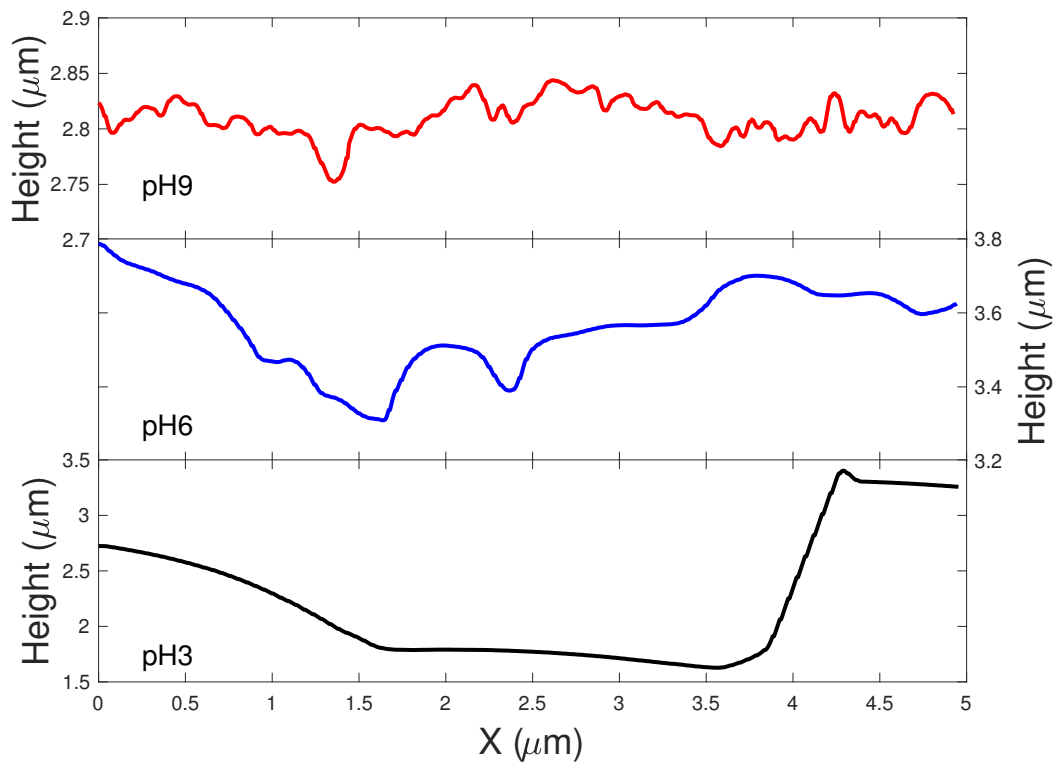


Figure 4: Line profile along the surface of the ELP samples produced at different pH values.

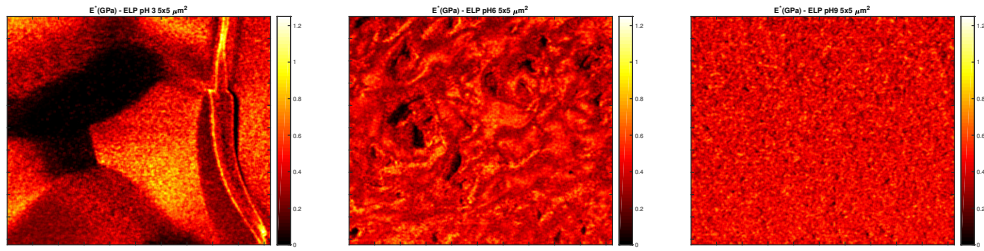


Figure 5: Maps of the elastic modulus  $E^*$  obtained fitting the force curves using the DMT model. Maps in panel a), b) and c) correspond to the scanned areas reported in Fig.3.

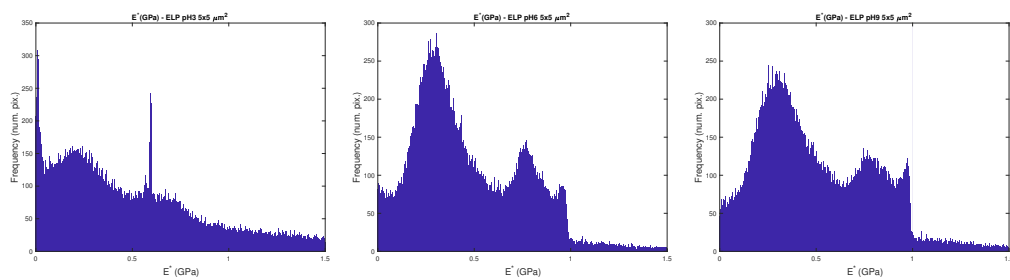


Figure 6: Histogram of distribution function of elastic modulus for ELP synthesized for different pH 3, 6 and 9

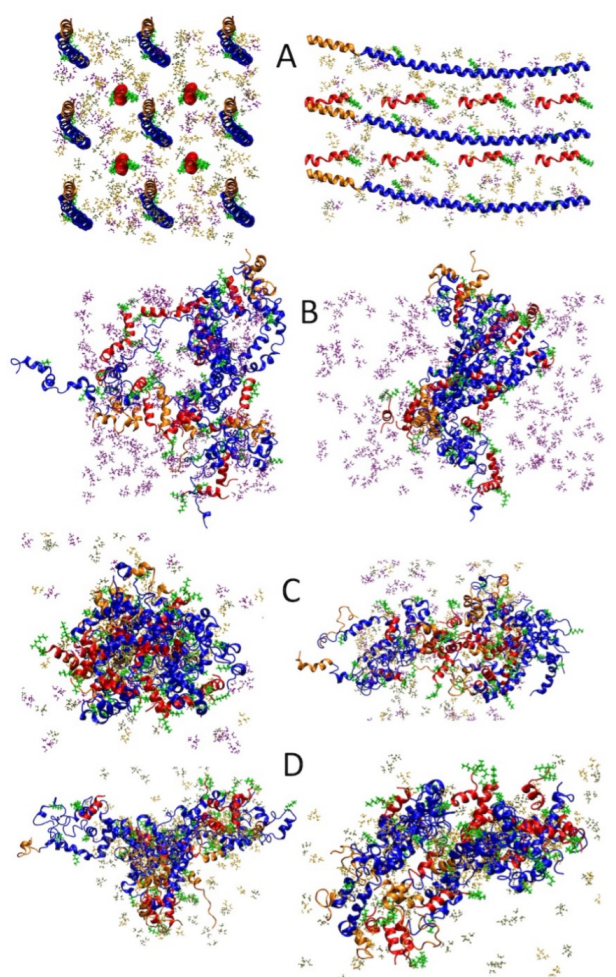


Figure 7: A) Top and B) side view of the initial configuration of the system for pH 7. The protein content and position are the same for all three pH value systems. The cell binding and structural binding sites are covalently connected. The initial configuration of proteins is set to  $\alpha$ -helical configuration. Cell binding peptides are in orange, structural binding peptides are in blue and QK peptides are in red. LYS amino acids are in green. THPC is in purple, TrHP is in orange and TrHPO is in tan.

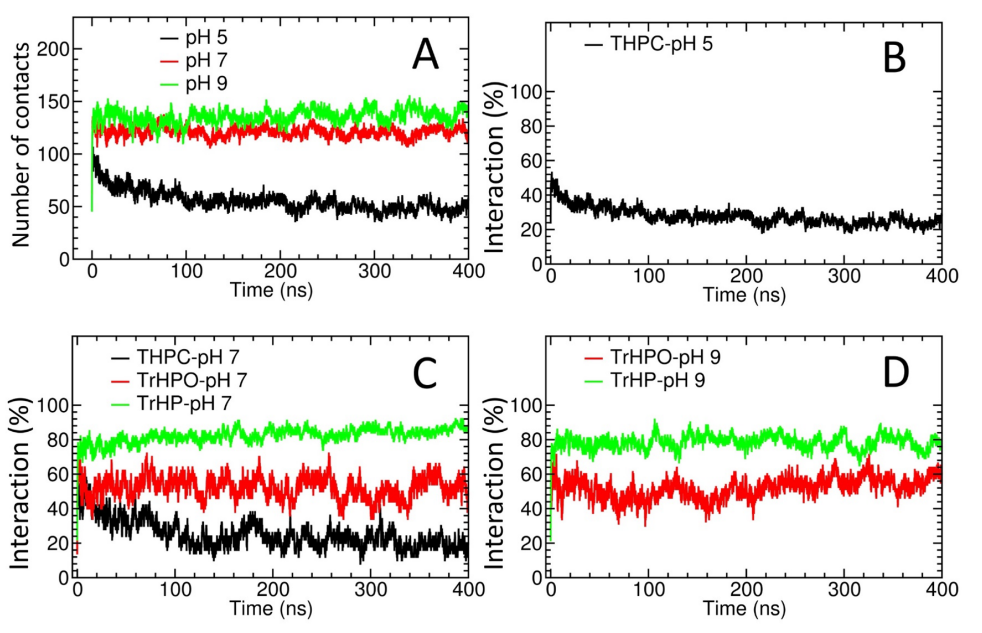


Figure 8: Interactions between the cross-linkers and proteins. A) Number of total contacts at different pH values, B) percent of THPC crosslinkers interacting with proteins at pH5, C) percent of different crosslinkers interacting with proteins at pH 7 and D) percent of different crosslinkers interacting with proteins at pH9.

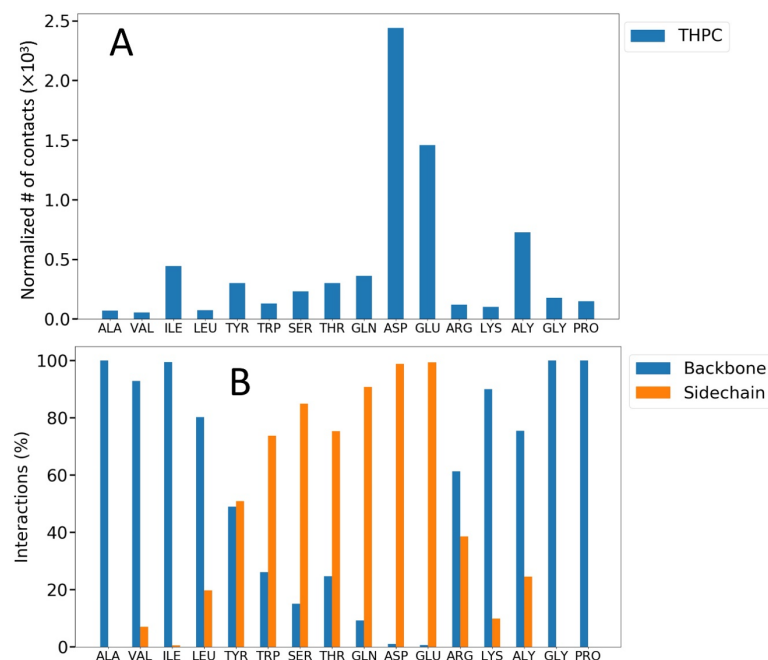


Figure 9: Cross-linkers at pH 5 interacting with different amino acids of the protein mixture. A) Number of contacts between THPC cross-linkers and different amino acids residues in the system and B) ratio of THPC interacting with the side chain vs backbone of each amino acid. The values in (A) are normalized by the number of amino acids in the system and the number of cross-linkers in the system.

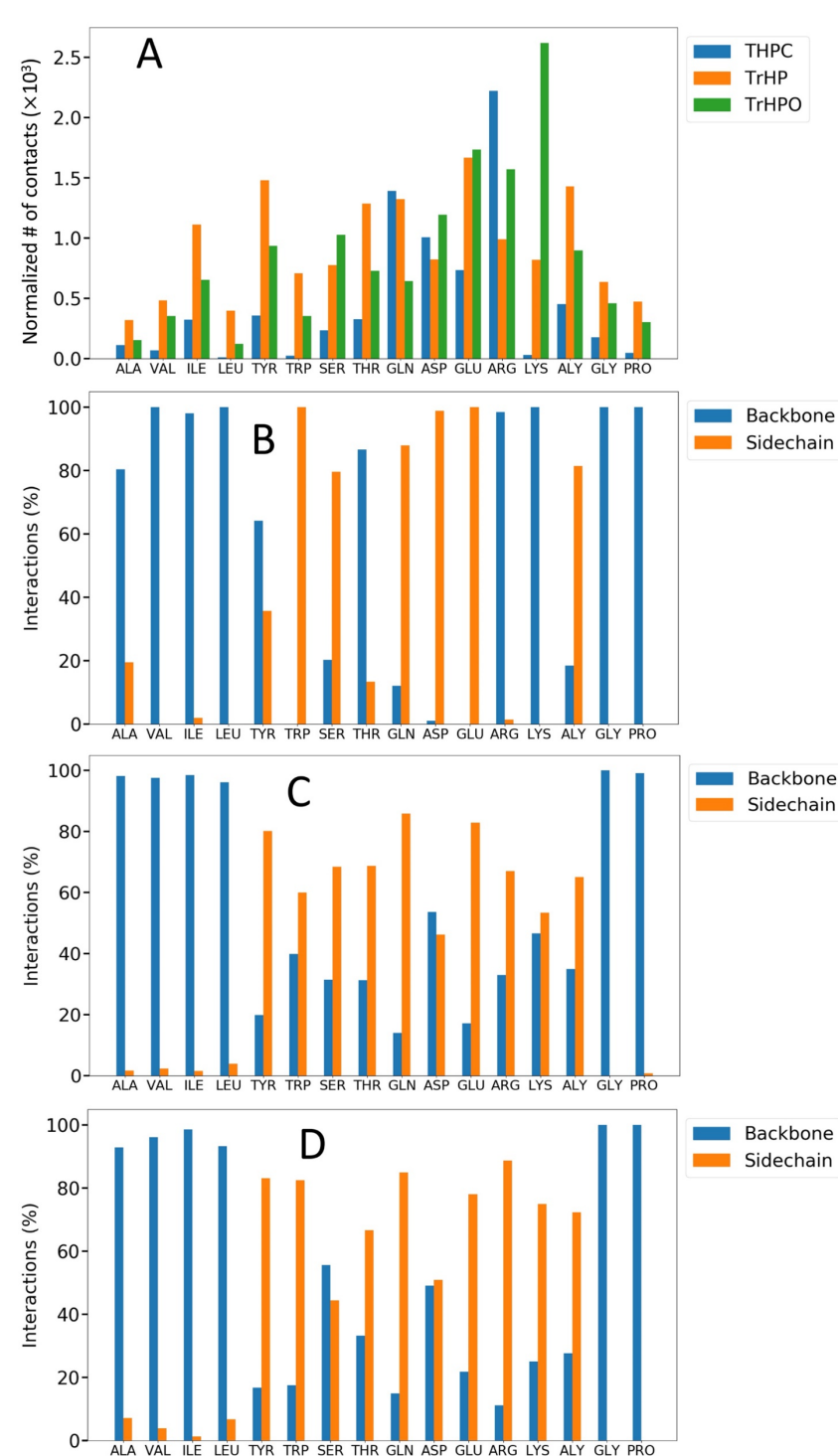


Figure 10: Cross-linkers at pH 7 interacting with different amino acids of the protein mixture. A) Number of contacts between THPC, TrHP and TrHPO cross-linkers and different amino acids residues in the system, B) ratio of THPC interacting with the side chain vs backbone of each amino acid, C) ratio of TrHP interacting with the side chain vs backbone of each amino acid and D) ratio of TrHPO interacting with the side chain vs backbone of each amino acid. The values in (A) are normalized by the number of amino acids in the system and the number of cross-linkers in the system.

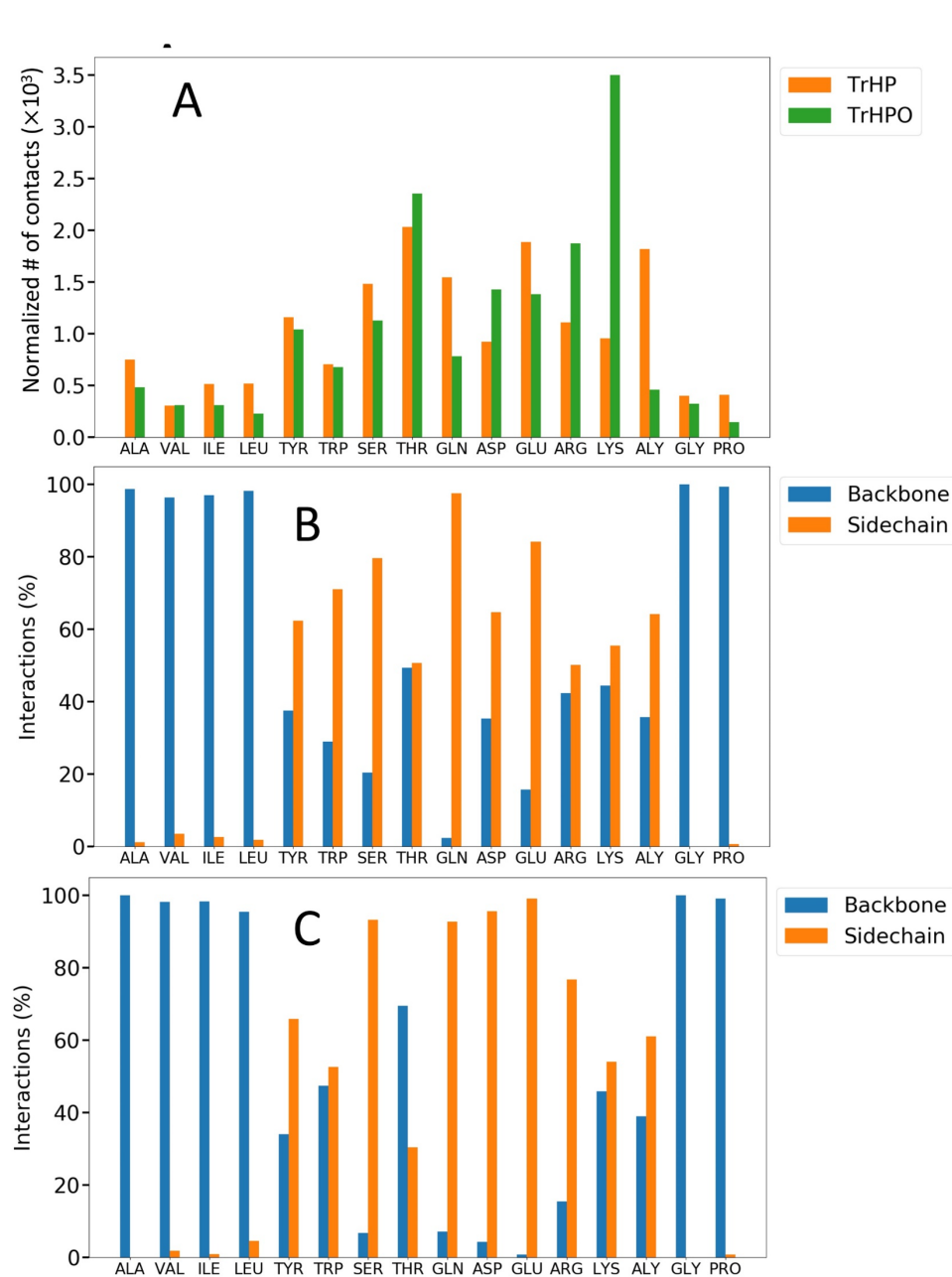


Figure 11: Cross-linkers at pH 9 interacting with different amino acids of the protein mixture. A) Number of contacts between TrHP and TrHPO cross-linkers and different amino acids residues in the system, B) ratio of TrHP interacting with the side chain vs backbone of each amino acid and C) ratio of TrHPO interacting with the side chain vs backbone of each amino acid. The values in (A) are normalized by the number of each amino acids in the system and the number of cross-linkers in the system.

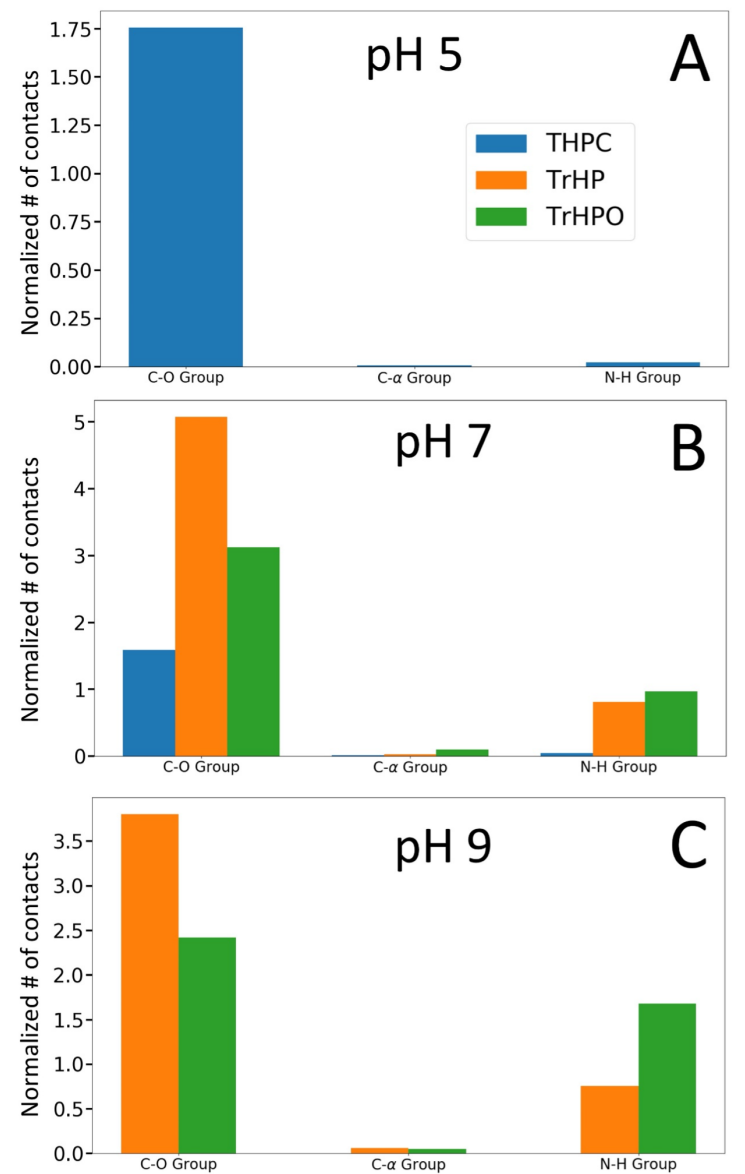


Figure 12: Number of contacts between different cross-linkers with different parts of protein backbone in different pH values. A) pH5, B) pH7 and C) pH9. Number of contacts are normalized by total number of the cross-linker.

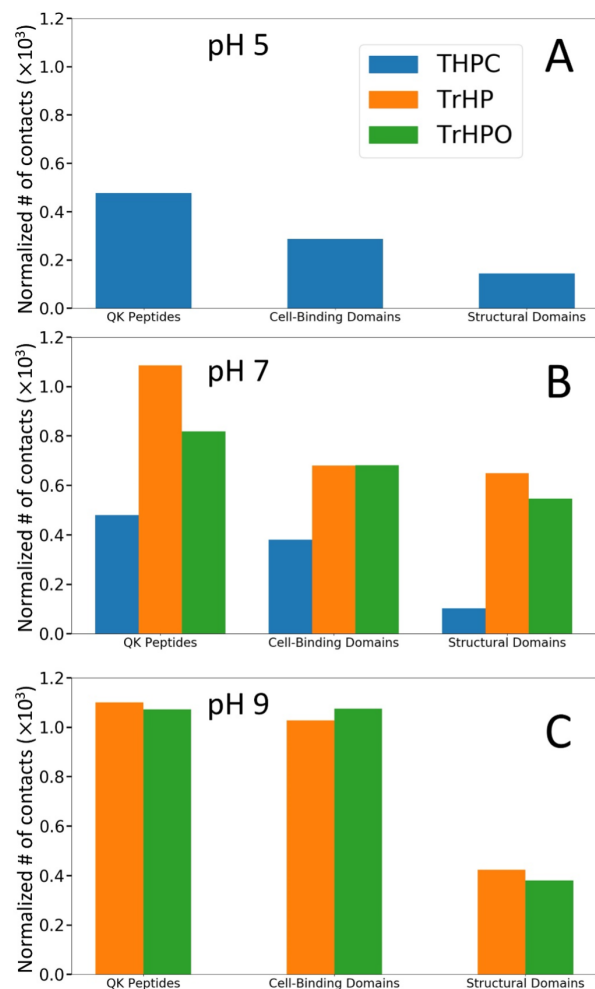


Figure 13: Number of contacts between different cross-linkers and different proteins in the system at different pH values. A) pH5, B) pH7 and C) pH9. Each cross-linker interaction is normalized by total number of the cross-linker. For each peptide, the number of interactions is normalized by number of the same type peptides, as well as the number of amino acids on each peptide.

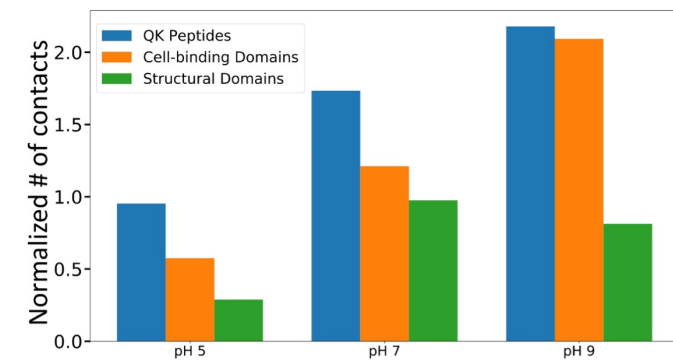


Figure 14: Number of contacts between all cross-linkers and different proteins in the system at different pH values. The values are normalized by total number of the cross-linkers and total the number of amino acids on each peptide.

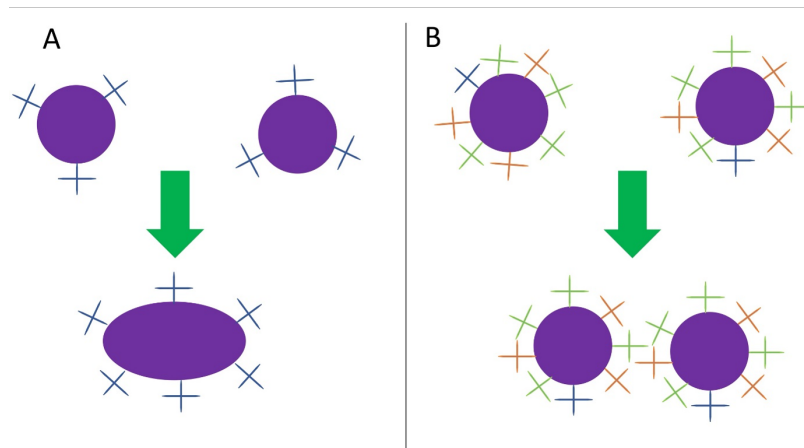


Figure 15: Schematics on the role of cross-linkers and proteins in producing the ELP configurations in different pH values. At low pH values (A), lower number of cross-linkers have covered the protein, while at higher pH values, (B) a greater number of cross-linkers have covered the protein. The aggregated proteins are shown as purple circles. The cross-linkers are shown as cross sign in different colors..